Universal MIMO-OFDM SDR for Mobile Autonomous Networks

FINAL REPORT

Nov. 24th, 2004

Office of Naval Research (ONR)

Issued by the U.S. Office of Naval Research Under

Contract No. N00014-04-M-0163

Name of Contractor: **Pulsar Communication Systems**
Project Scientist: **Dr. Babak Daneshrad**
Business Address:
3862 Kim Ln.
Encino, CA 91436
Phone Number: **(310) 738-1787**

Effective Date: **May 17, 2004**
Short Title of Work: **Universal MIMO-OFDM SDR for Mobile Autonomous Networks**
Contract Expiration Date: **Nov 24, 2004**
Reporting Period: **05/17/04 – 11/24/04**

Disclaimer

UNCLASSIFIED

Approved for public release; distribution unlimited

1. Introduction

This final report presents Pulsar's (Pulsar was recently incorporated as Silvus Communication Systems, Inc.) progress on NAVY SBIR topic number: N04-109, TITLE: Universal MIMO-OFDM SDR for Mobile Autonomous Networks. The report will present the findings of our phase-1 work and will provide an outline of work to be carried out under a possible pahse-2 contract.

Since the start of the work in late May, Pulsar has made significant progress towards the definition of a universal MIMO SDR architecture as well as the definition, simulation, and evaluation of the constituent algorithms and protocols that are needed to make the system a reality. The following three bullets summarize the main accomplishments of the phase-1 effort:

- A robust and highly agile software defined radio architecture has been identified along with a candidate set of algorithms that will enable end to end MIMO communications. These algorithms have gone through testing and verification.
- A complete end to end simulation has been created that implements all transmitter and receive algorithms in sample accurate simulation environment, and the resulting system performance has been simulated in characteristic environments. The results are quite positive and provide insight into the capability of both MIMO and the proposed architecture.
- Limited field trials using a non real time testbed have been carried out. In these trials, the simulation code was used to generate packets which were then transmitted in real time over the air. The receiver captured the transmissions and passed the received samples to the PC for processing. Over the air data rates of 160 Mbps were observed in typical indoor environments, with a small 1 mW TX power. Both indoor and outdoor stationary trials were carried out.

The initial field trials demonstrate the power of MIMO based communications and the flexibility of the Pulsar design. In fact during our field trials, we compared the performance of our MIMO OFDM testbed with a conventional 802.11a wireless LAN system. In indoor settings the MIMO system was able to deliver 40 Mbps of usable data at a distance of 200 feet, under the same exact operating and environmental conditions, the 802.11a system only delivered 2 Mbps to 4 Mbps of user throughput.

In our proposal, Pulsar presented a highly agile communication system that integrates Multiple Input Multiple Output (MIMO) techniques with Orthogonal Frequency Division Multiplexing (OFDM) in a software defined radio framework. These two techniques combined provide high throughput wireless communication that is resistive to harsh dispersive environments. Furthermore, spectrum agility is achieved by integrating a programmable RF front-end, digital IF sampling and controllable spectrum selectivity via direct digital frequency synthesis (DDFS). This enables the system to quickly transmission from one band of operation to another in order to mitigate interference or jamming.

The remainder of this report is organized as follows: Section two presents a brief review of the proposed SDR architecture and data flow. Section three presents the protocols and algorithms that we have studied and simulated for inclusion in the MIMO SDR. Section four provides the results from a preliminary set of experimental trials that incorporate the algorithms and protocols described in section three. Comparison of the results from these field trials with the simulations will provide a measure of the practical performance of the algorithms under real life settings. Section five, then concludes the report.

REPORT DOCUMENTATION PAGE

Form Approved
OMB No. 0704-0188

PLEASE DO NOT RETURN YOUR FORM TO THE ABOVE ADDRESS.

1. REPORT DATE *(DD-MM-YYYY)*	2. REPORT TYPE	3. DATES COVERED *(From - To)*
Nov 24, 2004	FINAL	From 5/17/04 to 11/24/04

4. TITLE AND SUBTITLE

Universal MIMO-OFDM SDR for Mobile Autonomous Networks

5a. CONTRACT NUMBER

N00014-04-M-0163

5b. GRANT NUMBER

5c. PROGRAM ELEMENT NUMBER

6. AUTHOR(S)

Ahmed Eltawil
Babak Daneshrad

5d. PROJECT NUMBER

5e. TASK NUMBER

5f. WORK UNIT NUMBER

7. PERFORMING ORGANIZATION NAME(S) AND ADDRESS(ES)

Pulsar Communication Systems
3862 Kim Lane
Encino, CA 91436

8. PERFORMING ORGANIZATION REPORT NUMBER

PUL003

9. SPONSORING/MONITORING AGENCY NAME(S) AND ADDRESS(ES)

Dr. Philemon Johnson, Dr. Santanu Das, Dr. Joel Davis
Office of Naval Research
800 North Quincy St.
Arlington, VA 22217-5660

10. SPONSOR/MONITOR'S ACRONYM(S)

11. SPONSOR/MONITOR'S REPORT NUMBER(S)

12. DISTRIBUTION/AVAILABILITY STATEMENT

Appoved for public release; distribution unlimited.

13. SUPPLEMENTARY NOTES

14. ABSTRACT

This final report presents Pulsar's (Pulsar was recently incorporated as Silvus Communication Systems, Inc.) progress on NAVY SBIR topic number: N04-109, TITLE: Universal MIMO-OFDM SDR for Mobile Autonomous Networks.
In the course of the Phase-1 effort Pulsar has defined a universal MIMO SDR architecture. We have also defined, simulated and evaluated all the constituent algorithms and protocols for the SDR. The following three bullets summarize the main accomplishments of the phase-1 effort:

- A robust and highly agile software defined radio architecture has been identified along with a candidate set of algorithms that will enable end to end MIMO communications. These algorithms have gone through testing and verification.
- A complete end to end simulation has been created that implements all transmitter and receive algorithms in sample accurate simulation environment, and the resulting system performance has been simulated in characteristic environments. The results are quite positive and provide insight into the capability of both MIMO and the proposed architecture.

15. SUBJECT TERMS

Wireless Communicatons; OFDM, Multi-Antenna Systems

16. SECURITY CLASSIFICATION OF:			17. LIMITATION OF ABSTRACT	18. NUMBER OF PAGES	19a. NAME OF RESPONSIBLE PERSON
a. REPORT	b. ABSTRACT	c. THIS PAGE			Babak Daneshrad
Unclassified	Unclassified	Unclassified	UU	28	19b. TELEPHONE NUMBER *(Include area code)* (310) 738-1787

INSTRUCTIONS FOR COMPLETING SF 298

1. REPORT DATE. Full publication date, including day, month, if available. Must cite at least the year and be Year 2000 compliant, e.g. 30-06-1998; xx-06-1998; xx-xx-1998.

2. REPORT TYPE. State the type of report, such as final, technical, interim, memorandum, master's thesis, progress, quarterly, research, special, group study, etc.

3. DATES COVERED. Indicate the time during which the work was performed and the report was written, e.g., Jun 1997 - Jun 1998; 1-10 Jun 1996; May - Nov 1998; Nov 1998.

4. TITLE. Enter title and subtitle with volume number and part number, if applicable. On classified documents, enter the title classification in parentheses.

5a. CONTRACT NUMBER. Enter all contract numbers as they appear in the report, e.g. F33615-86-C-5169.

5b. GRANT NUMBER. Enter all grant numbers as they appear in the report, e.g. AFOSR-82-1234.

5c. PROGRAM ELEMENT NUMBER. Enter all program element numbers as they appear in the report, e.g. 61101A.

5d. PROJECT NUMBER. Enter all project numbers as they appear in the report, e.g. 1F665702D1257; ILIR.

5e. TASK NUMBER. Enter all task numbers as they appear in the report, e.g. 05; RF0330201; T4112.

5f. WORK UNIT NUMBER. Enter all work unit numbers as they appear in the report, e.g. 001; AFAPL30480105.

6. AUTHOR(S). Enter name(s) of person(s) responsible for writing the report, performing the research, or credited with the content of the report. The form of entry is the last name, first name, middle initial, and additional qualifiers separated by commas, e.g. Smith, Richard, J, Jr.

7. PERFORMING ORGANIZATION NAME(S) AND ADDRESS(ES). Self-explanatory.

8. PERFORMING ORGANIZATION REPORT NUMBER. Enter all unique alphanumeric report numbers assigned by the performing organization, e.g. BRL-1234; AFWL-TR-85-4017-Vol-21-PT-2.

9. SPONSORING/MONITORING AGENCY NAME(S) AND ADDRESS(ES). Enter the name and address of the organization(s) financially responsible for and monitoring the work.

10. SPONSOR/MONITOR'S ACRONYM(S). Enter, if available, e.g. BRL, ARDEC, NADC.

11. SPONSOR/MONITOR'S REPORT NUMBER(S). Enter report number as assigned by the sponsoring/ monitoring agency, if available, e.g. BRL-TR-829; -215.

12. DISTRIBUTION/AVAILABILITY STATEMENT. Use agency-mandated availability statements to indicate the public availability or distribution limitations of the report. If additional limitations/ restrictions or special markings are indicated, follow agency authorization procedures, e.g. RD/FRD, PROPIN, ITAR, etc. Include copyright information.

13. SUPPLEMENTARY NOTES. Enter information not included elsewhere such as: prepared in cooperation with; translation of; report supersedes; old edition number, etc.

14. ABSTRACT. A brief (approximately 200 words) factual summary of the most significant information.

15. SUBJECT TERMS. Key words or phrases identifying major concepts in the report.

16. SECURITY CLASSIFICATION. Enter security classification in accordance with security classification regulations, e.g. U, C, S, etc. If this form contains classified information, stamp classification level on the top and bottom of this page.

17. LIMITATION OF ABSTRACT. This block must be completed to assign a distribution limitation to the abstract. Enter UU (Unclassified Unlimited) or SAR (Same as Report). An entry in this block is necessary if the abstract is to be limited.

2. Overall System Description

The top level functional block diagram of the Universal MIMO OFDM SDR is shown in Figure 1. Data is presented to a programmable dual band RF section employing a super heterodyne architecture which presents a low IF signal to the baseband data converters. The architecture does not suffer from the usual component matching, DC noise and flicker noise issues associated with direct conversion (zero IF) receivers.

Spectrum agility is achieved via a dual PLL+DDFS (direct digital frequency synthesizer) structure that provides the best of both worlds in terms of power efficiency and agility. The DDFS output is directly mixed with the VCO, thus providing the channelization required by the system. This is very beneficial since the DDFS can dial a new frequency in a fraction of the time required for a VCO based synthesiser to settle to the desired frequency (upwards of a few milli seconds). The combination of the two allows for quick hopping of +/- 100 MHz around the desired VCO carrier. Finally, the digital interpolating structure provides the means to implement a fully digital timing recovery loop by re-sampling the waveform and choosing the optimum sampling point that maximizes the received SNR.

Following a programmable length FFT operation, OFDM demodulation is performed for each antenna. Figure 2 shows the block diagram of the receiver for the proposed MIMO OFDM system, where each of the N receive antennas has P symbols corresponding to each OFDM sub-carrier. The effect of multipath propagation has been removed through the OFDM processing but the data is still corrupted by co-channel interference introduced by the simultaneous transmission from the M antennas. The MIMO channel corruption on the data is removed by applying MIMO decoding to the data received on the N receive antennas for each individual sub-carrier. The MIMO processing effectively inverts the MIMO channel and recovers the data transmitted from the M transmit antennas on each of the P sub-carriers. This process is applied to T consecutive MIMO OFDM symbols to obtain a block of MPT data corresponding to the blocks of PT data transmitted on the M antennas. Finally a serializer followed by a de-interleaver ($\prod_1^{-1}$) is applied to the data stream to obtain the bits to be delivered to the MAC layer.

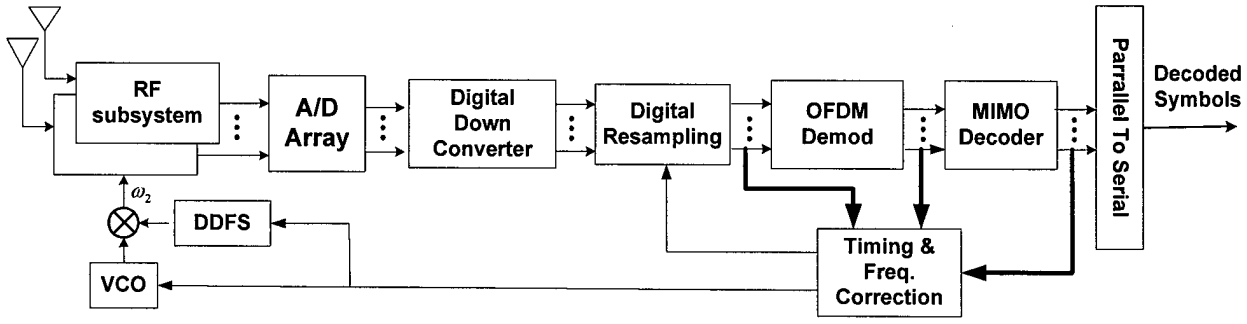

Figure 1, Top level receiver functional blocks for MIMO OFDM SDR

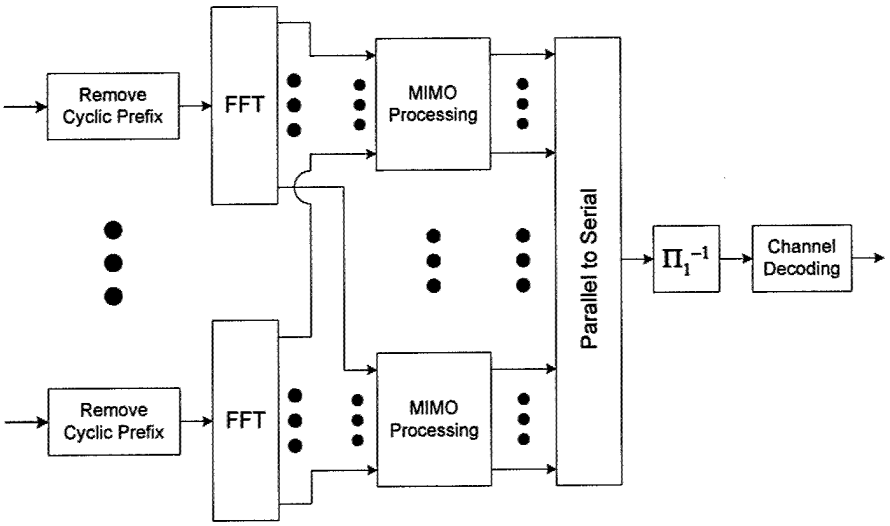

Figure 2. MIMO Receiver Block Diagram.

3. Protocol and Algorithmic Components

This section is devoted to providing a detailed description of the hardware blocks as well as the algorithms, protocols, and structures needed to actually realize MIMO transmission. Specifically, we will discuss the details of the OFDM modulator/demodulator, MIMO decoding, DDFS architecture, packet structure, the block boundary detection algorithm, the carrier frequency offset acquisition and tracking protocol, and the MIMO decoding approach.

OFDM

OFDM is a multi-carrier modulation scheme that has been developed for frequency selective fading channel environments [1]. OFDM modulates the data on orthogonal carriers, which are added and transmitted simultaneously. This effectively divides the wideband channel into a number of narrowband transmission sub-channels. A receiver can therefore be designed using lower complexity narrowband techniques on each sub-channel, which is important for a MIMO system. The use of Discrete Fourier Transform (DFT) for baseband modulation and demodulation allows efficient implementations by making use of the Fast Fourier Transform (FFT).

The OFDM modulator takes a block of P consecutive symbols *d(p)* and performs an inverse DFT (IDFT) to obtain the time domain sequence *d(t)* given by:

$$d(t) = \frac{1}{\sqrt{P}} \sum_{p=0}^{P-1} d(p) e^{j\frac{2\pi p}{P}}$$

A cyclic prefix is then pre-appended to the sequence as illustrated in Figure 3. The last L symbols of the IDFT output are pre-appended to the front of the IDFT output block. This creates a cyclic guard interval of length L, which prevents intersymbol (interblock) interference between consecutive OFDM symbols (blocks). The cyclic prefix also ensures orthogonality between sub-carriers when the signal is transmitted over dispersive channels. This guard interval between OFDM symbols must have a length L greater than the maximum excess delay expected from the channel to eliminate the ISI. Phase transitions at the boundary between consecutive OFDM symbols create spectral re-growth outside the signal bandwidth. To mitigate this effect, windowing of the OFDM symbols should be applied.

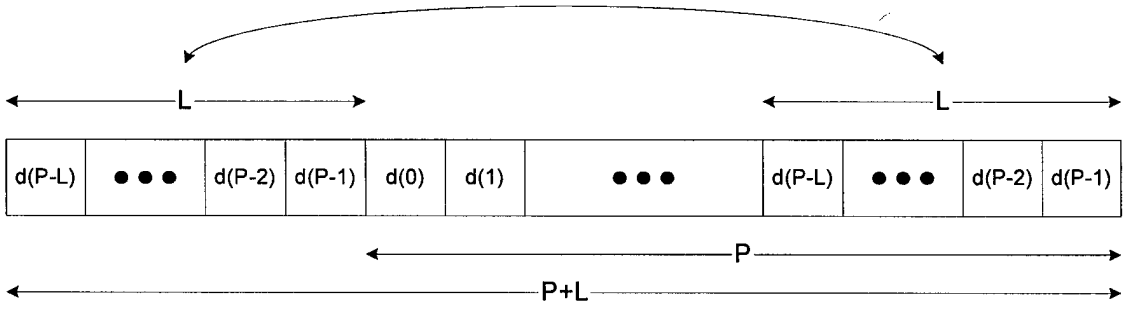

Figure 3. OFDM Cyclic Prefix

At the receiver, the OFDM boundary is identified through the initial synchronization and the first L symbols of each blocks of $P+L$ symbols are removed to obtain the sequence of P symbols $u(t)$. These symbols are not corrupted by the previous OFDM symbol (i.e., there is no OFDM symbol ISI) and due to the presence of the cyclic prefix, it can be shown that the sub-carrier orthogonality has been preserved. P consecutive receive samples $u(t)$ are then aggregated and sent through a DFT block. The DFT operation yields the channel output $u(p)$ for each sub-carrier p as follows:

$$u(p) = \frac{1}{\sqrt{P}} \sum_{t=0}^{P-1} u(t) e^{-j\frac{2\pi pt}{P}}.$$

Through the use of the frequency transforms, OFDM divides the broadband signal bandwidth into many orthogonal sub-carrier frequencies, Figure 4. Each orthogonal sub-carrier carries low data rates and can be treated as narrowband systems. The channel is therefore divided in the frequency domain into narrowband channels which allows OFDM to effectively combat harsh multipath propagation environments with a low-level of complexity compared to traditional single carrier equalized QAM schemes or even DSSS based CDMA schemes.

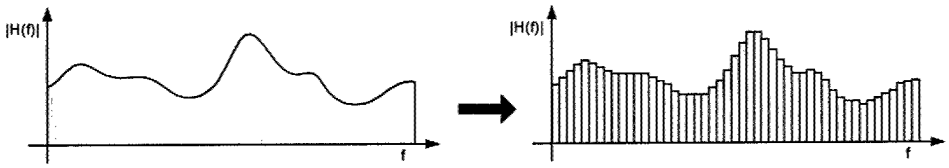

Figure 4. (left) A broadband single carrier system suffers from serious frequency selectivity and ISI. (right) OFDM divides the broadband signal into many smaller subcarriers, each of which sees a flat fading channel with no-ISI.

The number of subcarriers to be used is a function of the signal bandwidth and the coherence bandwidth which is equal to $B_c=1/2\pi\tau_{rms}$, where τ_{rms} is the average rms delay spread for the environment. Noting that any two subcarriers that have a separation of less than B_c are highly correlated, we can simplify some of the receiver processing by exploiting this fact. The channel correlation in the frequency domain can be exploited in OFDM by decreasing the number of sub-carrier transmitting pilots to estimate the channel and using interpolation to compute the channel estimates for the other sub-carriers.

MIMO

In recent years, numerous research projects [2],[3] have demonstrated the tremendous potential of MIMO technology for data communications. MIMO based wireless systems have the potential of increasing throughput by an order of magnitude or more without requiring any additional bandwidth. Fundamentally, a MIMO wireless system consists of M transmit antennas and N receive antennas whereas traditional systems only use a single transmit and a single receive antenna. The multiplicity of transmit and receive antennas increase the number of independent parallel communication channels available between the transmitter and the receiver which allows an increase in the channel throughput. The additional communication links also increase the channel diversity and improve the receive signal quality.

In addition to the increase in channel capacity, MIMO has several other interesting properties for military communication. For example, for a constant data rate, MIMO requires less transmit power therefore decreasing the probability of hostile entities detecting the transmission. Also, MIMO has some beamforming capabilities allowing the receiver to cancel an interference source. MIMO thus improves the anti-jamming performance of the communication system.

Since OFDM divides the wideband channel into P narrowband sub-channels, narrowband MIMO detection techniques are applied on each sub-carrier p to recover, from the data received on the N receive antennas, the data transmitted from each of the M transmit antennas. Several techniques can be used to perform narrowband MIMO detection, such as MMSE detection, VBLAST detection, and MMSE with cancellation detection. Pulsar is using an MMSE detector [11] to compute the estimate of the transmitted data. Define $\hat{D}(p)=\left[\hat{d}(p,1),\ldots,\hat{d}(p,M)\right]$, where $\hat{d}(p,m)$ is the estimate of the data transmitted on sub-carrier p from antenna m. $\hat{D}(p)$ is given by:

$$\hat{D}(p) = W(p)U(p)$$
$$= R_{u(p)}^{-1} R_{d(p)u(p)} U(p)$$
$$= \left(\frac{\sigma_d^2}{M} C_f^*(p) C_f(p) + R_{v_f(p)} \right)^{-1} \frac{\sigma_d^2}{M} C_f^*(p) U(p)$$

Where $R_{u(p)}$ is the auto-correlation matrix of the received vectors, $R_{u(p)d(p)}$ is cross correlation of the received vector and the desired signal, $C_f(p)$ is the channel response and $R_{vf(p)}$ is the auto-correlation matrix of the noise vector on sub-carrier p. σ_d^2 is the total transmit power which is kept constant as a function of the number of transmit antennas (in other words the sum of the powers transmitted on all antennas is maintained at the same value).

The weight matrix $W(p)$ can be obtained by estimating the channel state and directly computing the correlation matrices and their inverse. This approach requires a computationally intensive matrix inversion calculation. A different technique that can be used to avoid the matrix inversion is to use adaptive algorithms such as LMS or RLS. LMS has low computation complexity but has a slow convergence rate. RLS is slightly more complex but has a fast convergence and small steady-state error. Pulsar is proposing to use an RLS algorithm, which provides a good compromise between complexity and acquisition time, to compute the MIMO detector weight matrix.

Direct Digital Frequency Synthesis

Direct Digital Frequency Synthesis is an indispensable technique for generating reference frequencies whenever extremely precise frequency resolution and fast switching speeds are required. The most common DDFS architecture is the Tierney, Rader, Gold architecture [4]. This architecture, which has been well documented in the literature [5][6], [7] synthesizes a sine wave by using a periodically overflowing phase accumulator to generate and store phase information, and uses a ROM based look-up table to compute the sine function, as shown in Figure 5. The frequency of the generated sinewave is controlled by the Frequency Input Word (FIW) as shown by the following equation.

$$f_{\min} = \frac{f_{clk}}{2^L}$$
$$f_{out} = f_{\min}.FIW$$

Where f_{min} is the minimum synthesizable frequency, f_{clk} is the clock frequency, L is the word length of the phase accumulator, f_{out} is the output frequency and FIW is the frequency input control word.

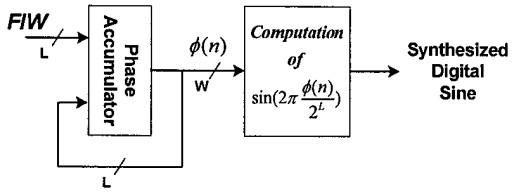

Figure 5 DDFS Architecture

Optimization of the DDFS architecture involves trading off finite word lengths and the sine computation methods against the sine-wave spectral purity and maximum clock rate. ROM compression techniques are essential, since a straight forward implementation of the sine function look-up table requires more than 4 Giga samples of storage for a phase accumulator resolution of 32 bits and output resolution of 12 bits. However, compression techniques inevitably lead to degradation in the spectral purity of the generated sine wave. Pulsar has performed a survey of available compression techniques and DDFS architectures. The most common of which is a technique that takes advantage of the sine and cosine symmetry. This compression technique makes use of the fact that the sine wave from $\pi/2$ to $\pi/4$ is the same as the cosine from zero to $\pi/4$, and the cosine wave from $\pi/2$ to $\pi/4$ is the same as the sine from zero to $\pi/4$. This means that only one-eighth of sine and cosine functions (from zero to $\pi/4$) are stored in the ROM.

Packet Structure

The packet structure is by far the most fundamental part of the system specifications. The structure of the packet will impact the algorithms to be used at the receiver as well as the performance demanded of those algorithms. Consequently, one of the first issues addressed by the Pulsar team was to solidify the packet structure to be used in our system. Implicit in this is that the developed system will be a packet based (as opposed to a circuit switched). Each packet is assumed to be unique and independent. No prior information about the channel state is assumed from prior transmissions. With the onset of each packet, the system is initialized from scratch and all parameters estimated.

Figure 6 shows a time-frequency plot of the packet structure. Along the frequency axis are the subcarriers and along the time axis are the individual OFDM blocks. Some subcarriers at DC and at the band edges are unused (to accommodate hardware filters), this is a programmable parameters in the SDR so as to allow the user to interface the baseband to any RF subsystem, and as such increase the utility of the final MIMO SDR.

As shown in the figure, some subcarriers are dedicated as synchronization pilots. These are continuous pilots used to estimate and track carrier frequency and timing offset. The number of pilot subcarriers is related to the coherence bandwidth of the channel and the bandwidth of the transmitted signal. Three to four pilots equally spaced at integer multiples of the coherence bandwidth has been shown to provide good performance. The structure of the pilot sequence itself is not very critical, as long as it is predictable at the receiver, the system will be able to lock onto it and track it. It is preferable to have these pilots be pseudo-random and transmitted at a slightly higher power level. This holds true for both SISO and MIMO based systems and is the approach taken in the development of our MIMO SDR platform.

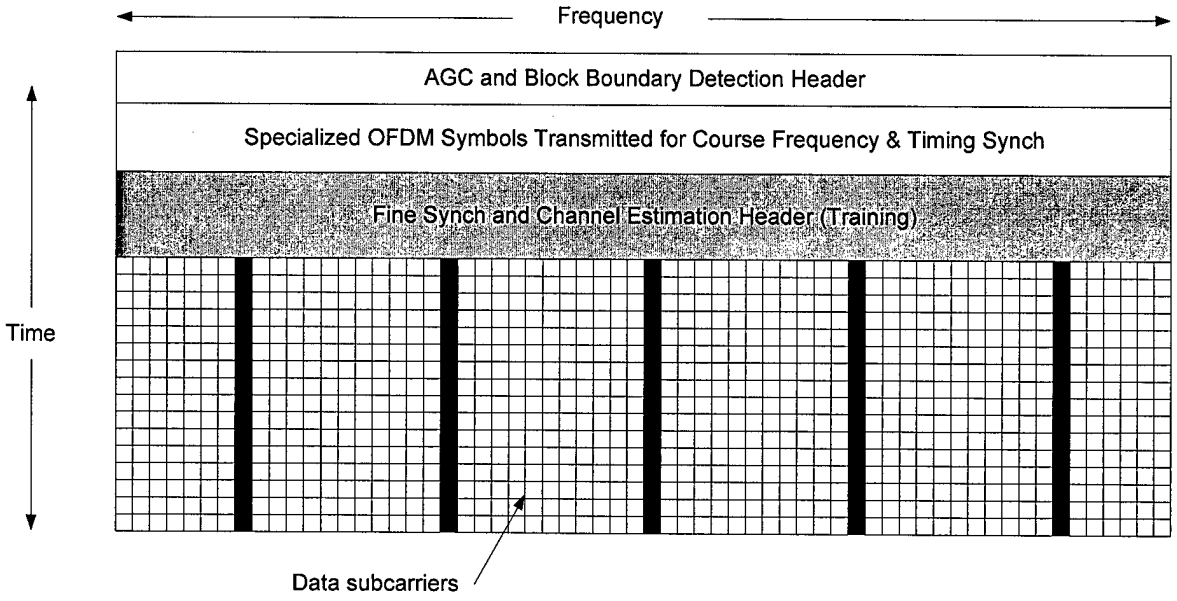

Figure 6. A time-frequency plot of the packet structure

Referring to Figure 6 the first OFDM block in each packet is used for block boundary detection (also referred to as acquisition or ACQ for short). This operation is analogous to symbol timing synchronization in conventional single carrier systems. Since OFDM is a block operation, the receiver must know the onset of a block so that it can assemble the entire block prior to sending it off to the FFT unit for demodulation. There are many approaches for acquiring the block boundary. Some require a certain symmetry in the acquisition header, while others require a pseudo random signature sequence. We investigated both approaches and decided in favor of the former due to its ease of implementation and acceptable performance per our simulations.

The second field is a rather short field used for course timing and frequency estimation, although at this stage improving the carrier frequency estimate is more important than improving timing estimates. This is due to the sensitivity of OFDM to carrier frequency offset. Additionally it is important to correct as much of the carrier frequency offset ahead of the channel estimation (training) phase. The channel estimation processing assumes a reasonable frequency lock. Given that the SDR will be used in different environments and operating conditions, this field is highly parameterizable. The user can specify the length of this field as well as the number of subcarriers to be used.

The next field in the packet structure is the channel estimation (training sequence) field. This field is used to learn the channel state information which includes the channel impulse response, the noise power going into the receiver and the presence or absence of any interferers. It is desired to design this field in con junction with the channel estimation algorithm. So that techniques could be developed that would help estimate all three elements of the CSI simultaneously, or alternatively develop algorithms at the receiver that do not require each piece of information explicitly, but rather can work on the estimate of the signal plus noise and interference. This is in fact what the Pulsar team finally converged on. The converse would have required a training header which would have consisted on three distinct fields and would have been too long to be practical, specially for short packets.

The final field of the packet structure is the data blocks. There is more here than meets the eye, since as an SDR the unit requires many different options for programmability. As the environment within which the radio is to operate changes from indoor, to outdoor urban, to outdoor forested, etc, the delay spread changes and it is necessary to change the number of subcarriers that the modem can use for communications. As a result we have introduced the requirement for variable number of subcarriers, and a user defined M-QAM constellation for data transmission.

Now that the specific fields within the packet structure have been defined, it is worth noting the level of user programmability that is available in the system. In the proposed SDR, the user has full control over the number and configuration of the antennas to be used, the number of subcarriers, the constellation size, the amount of cyclic prefix, the number of pilots and the training overhead Table 1 lists all the parameters programmable in the packet structure. In addition there are other parameters and controls that are part of the configuration script that can turn on or turn off specific features. Prominent among them are the ability to turn off synchronization algorithms when operating in perfect-timing mode, control over phase noise cancellation and control over block shaping feature including the shape of the window function.

Table 1, List of all parameters in the packet structure

Number of transmit antennas (M)	1 to M
Number of receive antennas (N)	1 to N
Number of subcarriers (NFFT)	64, 128, 256, 512, 1024
Constellation size	4, 16, 64
Training blocks (BTRAIN)	Variable depends on MIMO configuration
Data blocks (BDATA)	Variable, depends on the coherence time
Continuous pilots(CPN_PILOTS)	Variable,
Cyclic prefix(CPRE)	Variable depending on the channel delay spread
Cyclic postfix(CPOST)	Variable depending on the channel delay spread
Lower band unused subcarriers (UNUSEDLOW)	Variable
Upper band unused subcarriers (UNUSEDUPP)	Variable
Unused positive DC subcarriers (NODCP)	Variable
Unused negative DC subcarriers (NODCN)	Variable

COMMUNICATION SYSTEM DESCRIPTION

The Pulsar MIMO SDR is a packet mode communication system. The block diagram of a spatial multiplexing MIMO-OFDM system is shown in Figure 7 and Figure 8. The data bits are multiplexed onto independent OFDM modulators, each of which drives a transmit antenna. Each of the OFDM modulators map the data bits to a QAM constellation, an IFFT operation transforms this frequency domain data into the time domain where a cyclic prefix and postfix are added. The data is upsampled and filtered prior to being sent over the air. In the case of the simulated system, data is written into a file, referred to as the transmit vector, after being upsampled and filtered.

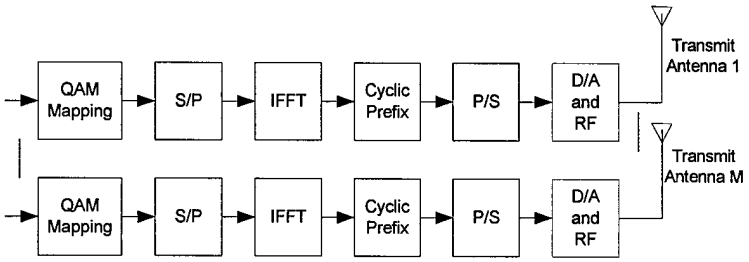

Figure 7 Transmitter of a MIMO-OFDM system

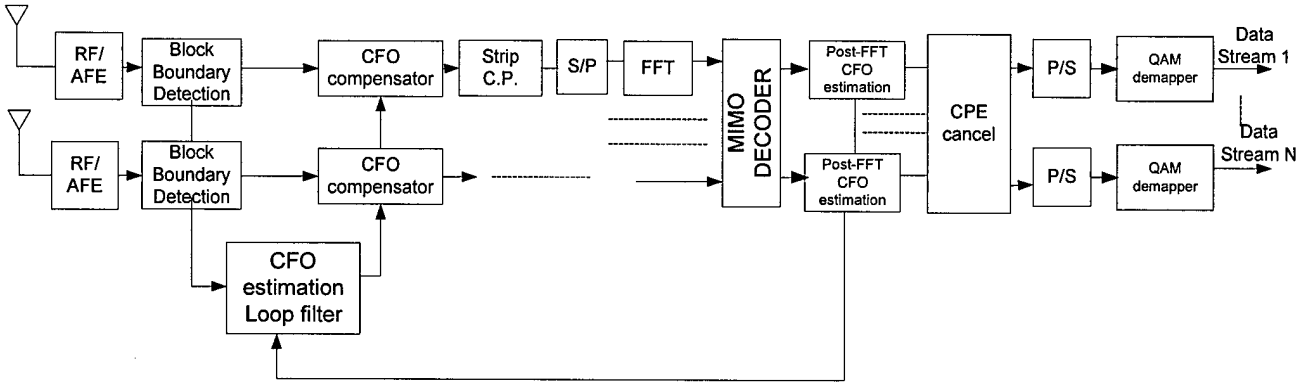

Figure 8 Receiver of a MIMO-OFDM system

During simulation, the channel module reads the samples written out by the transmitter, generates random multi-path fading channels and convolves the transmitted data with the MIMO channel and writes the resulting vector into a file, referred to as the channel output file.

The receiver module reads the file generated by the channel module. First all the receiver impairments are added such as carrier frequency offset (CFO), sampling frequency offset (SFO), AWGN, phase noise, etc. The first step in the MIMO-OFDM demodulator is the block boundary detection (also known as

timing acquisition). A block boundary detection algorithm working on the received samples and detects the FFT block boundary. The frequency offset compensator corrects for carrier frequency offset. This is followed by stripping the cyclic prefix on the data streams at each of the receivers. At this point the post-FFT algorithms kick in. An FFT operation transforms the data into the frequency domain and a MIMO decoder operating on each of the subcarriers extracts each of the transmit data streams. Next, the post-FFT CFO estimation algorithm, phase noise cancellation algorithms and the IQ mismatch correction algorithms are executed.

BLOCK BOUNDARY DETECTION (TIMING ACQUISITION)

The first few OFDM blocks in the packet are used for block boundary detection, also known as timing acquisition. This scheme requires many OFDM symbols (the acquisition preamble) specifically designed for acquisition. Each of the OFDM symbols in the time domain have identical data in the first half of the block (symbol) and the second half of the block. The last block in the preamble has the data inverted. The same acquisition block is used at all the transmitters, thereby ensuring higher power for the block boundary detection preamble.

The block boundary detection module at the receiver compares each of the received blocks to see if the first half of the block is identical to the second. When there is a match the block boundary acquisition module registers a peak. When the series of positive peaks are followed by a negative peak block boundary is detected. This is depicted in Figure 9 below. The symmetric nature of the OFDM blocks used for block boundary detection are shown in the Figure, the symmetric (in the time domain) blocks are self correlated to produce the peaks shown in the lower half of the figure. At the receiver the unit simply performs a self correlation of the incoming sample stream and counts the number of positive correlation peaks prior to receiving a negative correlation peak.

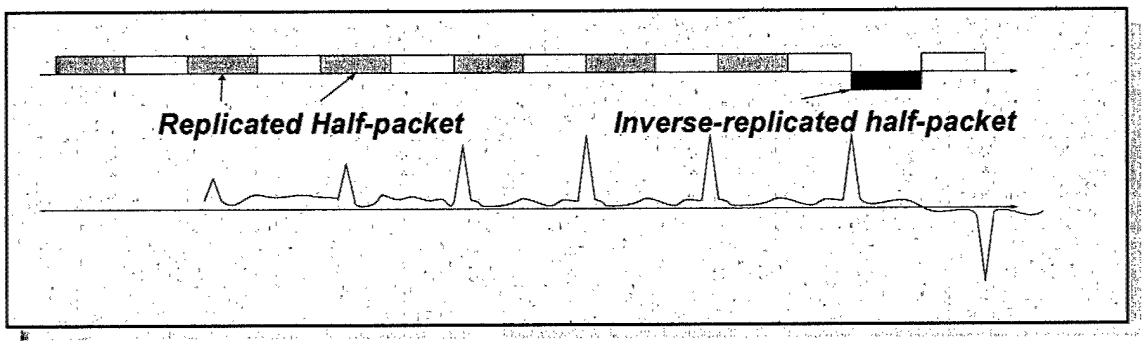

Figure 9, block boundary detection

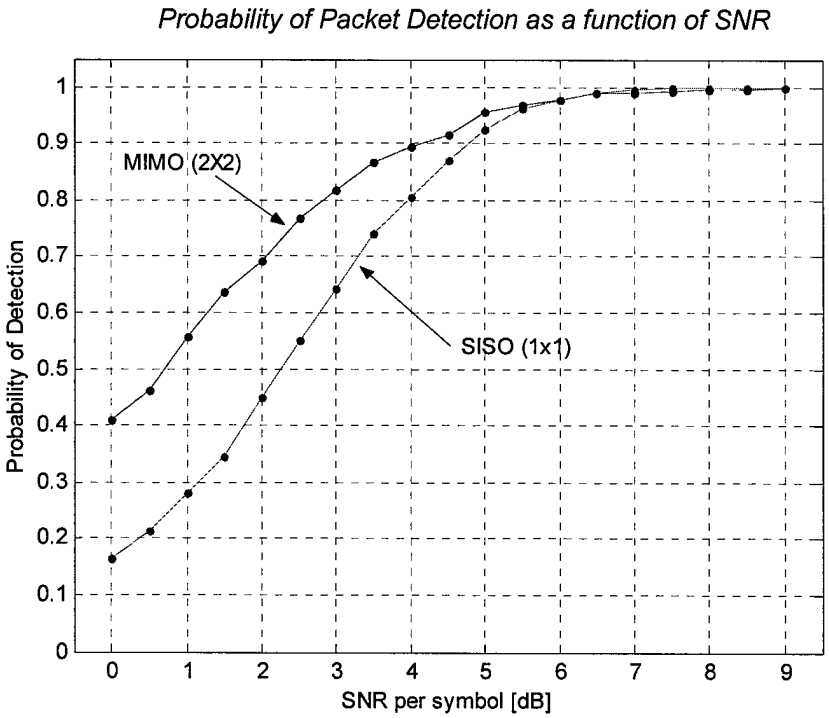

Figure 10, Probability of packet detection vs. SNR for both a SISO and a MIMO system

It is commonly accepted that a self correlating block boundary detection is inferior to a scheme whereby the signature sequence is correlated with a pre set sequence known at the receiver. This is a well established fact as the correlation results do not suffer from double noise that is introduced in self correlating type detectors. However, what is important is that the detection must be reliable within the SNR range of operation. Figure 10 shows the result of simulation conducted to determine the probability of detection for the proposed block boundary detection protocol. As can be seen there, the detection probability is above 95% with only 5 dB SNR. It climbs to almost 100% when the input SNR is increased to 7 dB. This is the lower range of acceptable operating SNRs. The plot also shows the improvement in detection probability obtained with a small 2x2 MIMO system.

CARRIER FREQUENCY OFFSET SYNCHRONIZATION AND TRACKING

Carrier frequency offset (CFO) causes a constant rotation of the constellation on all the subcarriers which increases from one MIMO-OFDM block to the next. This is shown in Figure 11 where the constellation on a given OFDM subcarrier is seen rotating from one block to the next block along the time axis. The amount of rotation is proportional to the CFO and the duration of each OFDM block. The CFO in OFDM systems is generally normalized by the subcarrier spacing and is separated into an integer part and a fractional part. The integer part indicates the number of subcarriers the carrier frequency is shifted

by and the remainder is termed the fractional part. The fractional part causes intercarrier interference (ICI) in which case the data being transmitted on neighboring subcarriers start to interfere with one another. This is analogous to the problem of intersymbol interference (ISI) in conventional single carrier QAM systems.

Both pre-FFT cyclic prefix based methods and post-FFT methods can be used to compute the fractional part of the CFO (when the CFO is less than half the subcarrier spacing). However, post-FFT algorithms are needed to detect the integer part of the CFO. Estimating the integral part can be avoided if the CFO is guaranteed to be within half the subcarrier spacing.

The fractional part of the CFO can be estimated by examining the phase rotation in the frequency domain (post-FFT) or in the time domain (pre-FFT). The carrier frequency offset is compensated in the receiver by applying a linearly increasing rotation equal to the CFO estimate, on each of the received samples. The post-FFT estimator is based on measuring the angular rotation on the subcarriers from one OFDM block to the next and requires continuous pilots.

Each of the subcarriers of an OFDM block is rotated by the same amount in the presence of the CFO. The amount of angular rotation from one OFDM block to the next is proportional to the CFO. Pilots are used to compute the angular rotation on each of the subcarriers of one OFDM block and subsequently the angular rotation from one block to the next is computed. The CFO estimate is based on the average of the angular rotation on all the pilot subcarriers and then averaged across all the transmit data streams. The estimate of CFO is then passed thru a simple first order loop filter before feeding back to compensate for CFO on the next OFDM block. This scheme can be used both for CFO acquisition as well as tracking the CFO (after initial acquisition). Tracking will require continuous pilots or pilots at regular intervals.

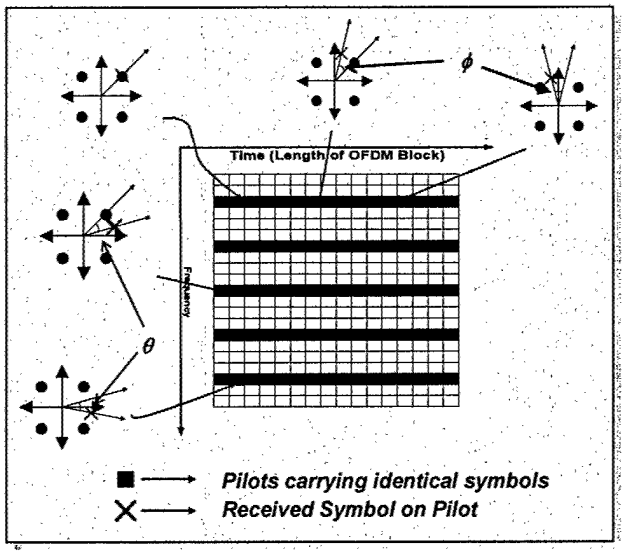

Figure 11, Effects of carrier frequency offset and timing frequency offset on an OFDM system employing QPSK modulation on each subcarrier. CFO will cause a rotation of the constellation in time on the same subcarrier. Timing frequency offset will cause a rotation of the constellation in frequency within a given block.

A coarse estimate of CFO is available with block boundary detection. This estimate is refined by using the cyclic prefix based CFO estimator. However, when RLS training of W_k is on, after W_k is trained a more robust post-FFT estimator is used for tracking the CFO. The post-FFT estimator is based on measuring the angular rotation on the subcarriers from one OFDM block to the next, Figure 11, and requires continuous pilots. Two different schemes are needed because the feedback loop in the post-FFT CFO compensation scheme interferes with the RLS training of W_k.. The first scheme is a time domain scheme based on the cyclic prefix correlation, and the second scheme is a frequency domain (post-FFT) estimator based on the continuous pilot signals.

A block diagram of the CFO estimation scheme based on cyclic prefix correlation is shown in Figure 12. This scheme correlates the received samples spaced N_s apart, where N_s is the number of subcarriers. When the cyclic prefix of the OFDM symbol falls in the correlation window the samples being correlated are exactly identical except for a phase rotation which is proportional to the CFO. An estimate of the CFO is available by dividing the angle of the correlation sum by $1/2\pi$. In a MIMO-OFDM system this estimation algorithm is executed on the data streams from each of the receive antennas. The estimate of the CFO from one OFDM block is computed by averaging the CFO from each of the received data streams. This estimate is passed thru a simple first order loop filter before applying a corrective rotation to compensate for the CFO. The cyclic prefix based CFO estimation algorithm is continuously executed on all the OFDM training symbols when the channel inverse estimator is being trained. This is because the RLS training algorithm conflicts with the more robust post-FFT CFO estimation algorithm that feeds back the CFO estimate from the past OFDM blocks to correct the CFO of the current OFDM block. The performance of the cyclic prefix based estimation algorithm is directly related to the length of the cyclic prefix.

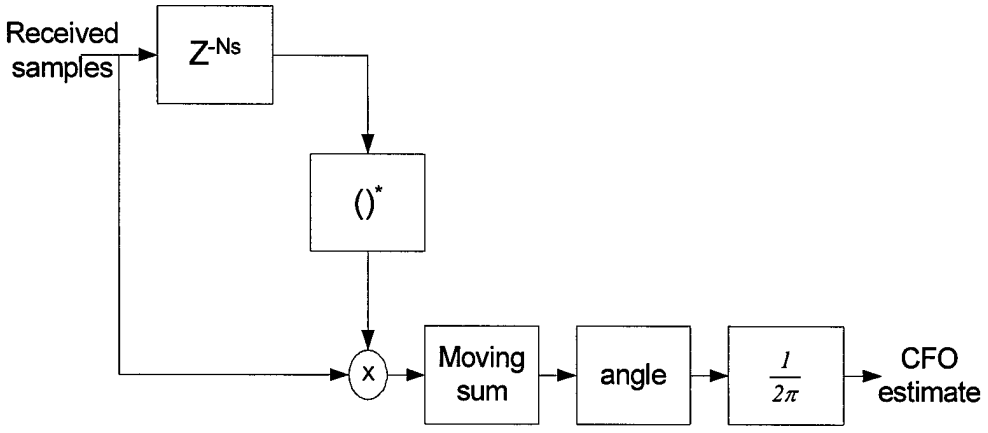

Figure 12, A CFO estimation scheme based on cyclic prefix correlation

The post-FFT based carrier frequency offset estimator requires pilots for estimating the CFO (unlike the cyclic prefix based scheme). Each of the subcarriers of an OFDM block is rotated by the same amount. The amount of angular rotation from one OFDM block to the next is proportional to the CFO.

Pilots are required to compute the angular rotation on each of the subcarriers. If $\hat{X}_n(k)$ and $\hat{X}_{n+1}(k)$ indicate the estimates of the transmitted symbols on the k^{th} subcarrier for OFDM symbol n and $n+1$ respectively from all the transmit antennas, the angular rotation between these two symbols caused by CFO $e^{j\frac{2\pi\varepsilon_c(N_s+N_{CP})}{N_s}}$ is . N_s is the number of subcarriers and N_{CP} is the number of samples in the cyclic extension (cyclic prefix + cyclic postfix). ε_c is the CFO normalized to the subcarrier spacing. To estimate the CFO, the outputs of the MIMO decoder of all the transmit data streams on the k^{th} subcarrier are multiplied by $\hat{C}_n^*$ and $\hat{C}_{n+1}^*$ the conjugate of the pilots on those subcarriers.

To compute the angular rotation between the two consecutive blocks $Z_n(k)$ is used

$$\theta(k) = \angle Z_n(k) Z_{n+1}^*(k) = \frac{2\pi\varepsilon_c(N_S + NCP)}{N_S} \qquad (0.1)$$

for all pilot subcarriers, k

The average of the angular rotation on all the subcarriers and all data streams is used to compute the estimate of the CFO.

$$\hat{\varepsilon}_c = \frac{mean(\theta(k))}{2\pi(1+\frac{N_{CP}}{N_S})} \qquad (0.2)$$

The mean in (0.2) is the average of the angular rotation on all the pilot subcarriers and the average across all the transmit data streams. The estimate of CFO, $\hat{\varepsilon}_c$ is then passed thru a simple first order loop filter before feeding back to compensate for CFO on the next OFDM block. This scheme can be used both for CFO acquisition as well as tracking the CFO (after initial acquisition). Tracking will require continuous pilots or pilots at regular intervals in time on some of the subcarriers. Most of the popular wireless LAN standards provide dedicated pilot subcarriers for CFO estimation and tracking. The performance of this algorithm depends on the number of pilot subcarriers available for CFO estimation.

MIMO DECODING

Following block boundary detection, the post-FFT algorithms are initiated. There is a MIMO decoder at the receiver that recovers the transmitted vector from the received vector. The output of the FFTs on each antenna branch is input to the MIMO decoder. The MIMO decoder requires channel state information which require the training symbols embedded in the packet. After the channel impulse response has been estimated the channel inverse is obtained which when multiplied with the received symbol vector on each subcarrier, extracts the transmitted data vector.

Adaptive techniques like LMS and RLS can be used to iteratively compute the weight matrices avoiding expensive matrix inversion operations. These rely on training symbols but provide a low complexity method to compute the optimal weight matrix W_{opt}. Derivations of the LMS and RLS algorithms can be found in [11].

The LMS algorithm (also known as the Widrow-Hoff algorithm) is

$$W_i = W_{i-1} + \mu[X_i - W_{i-1}Y_i]Y_i^*$$
$$E_i = [X_i - W_{i-1}Y_i]$$
$$W_i = W_{i-1} + \mu E_i Y_i^*$$

μ is the step size. E_i is also known as the a-priori error at iteration i.

The LMS algorithm is popular for its simplicity and low computational complexity. However, depending on the step-size μ it might require a large number of "training symbols" to converge to the optimal weight matrix W_{opt}. This could be detrimental in packet mode communication systems because the training symbols are overheads that reduce the "user data rate". The RLS algorithm requires far fewer training symbols to converge but also has much higher complexity [11].

AGC

The automatic gain control (AGC) circuit is rather straight forward. Our approach is to have the AGC function carried out in the baseband by monitoring the signal just after the data converter. The in-phase and quadrature signals are squared and then summed to provide the instantaneous power in the received signal. This is then summed in a running average operation to produce an estimate of the incoming power which is then compared to a threshold to produce an error signal. The error signal is then further averaged in an integral plus proportional loop filter before getting fed back to the variable gain amplifier (VGA). The one major issue that needs to be dealt with in the AGC loop is a mapping of the error signal to the proper VGA control voltage. This is typically a non-linear operation and requires a series of calibration measurements to be conducted on the VGA circuit itself. The resulting mapping will be stored in a table for use in the AGC loop.

Performance Results

Idealized MIMO Capacity Results

Having completely defined the packet structure, and the algorithms to be used in the receiver, the Pulsar team initiated the process of quantifying the performance of the end to end system in a series of simulations. In these studies, the packet structure as defined above was fully implemented. Moreover, all relevant algorithms were also included. The channel was modelled as having an exponential power delay

profile with variable rms delay spread. In our studies the rms delay spread was chosen to be on the same order as the reciprocal of the signal bandwidth. The cyclic prefix was chosen sufficiently long so as to guarantee orthogonality of the OFDM subcarriers even in the most dispersive of channels (note that a channel with an rms delay spread of τ_{rms} may have multipath components as far away as $8\tau_{rms}$).

Figure 13 shows the complementary cumulative distribution function (CCDF) of a MIMO 4x4 system as a function of the Rician K factor of the channel. The Rician K factor measures the relative strength of a line of sight path to the Rayleigh fading non-line of sight paths. As K is reduced, the channel becomes more Rayleigh like, and as K is increased, the line of sight term in the channel becomes more and more dominant and the channel becomes more AWGN like than Rayleigh. The curves underscore the generally anticipated trend that the capacity of MIMO systems increase as the LOS component of the channel dies out. The significance of the curve is that it actually quantifies this trend, and more over it models a realistic (as compared to an idealized) receiver. Per the results of Figure 13, the MIMO system described in this report can deliver as much as 22 bps/Hz of capacity under conditions with minimal implementation loss. This condition will be relaxed in follow on discussions.

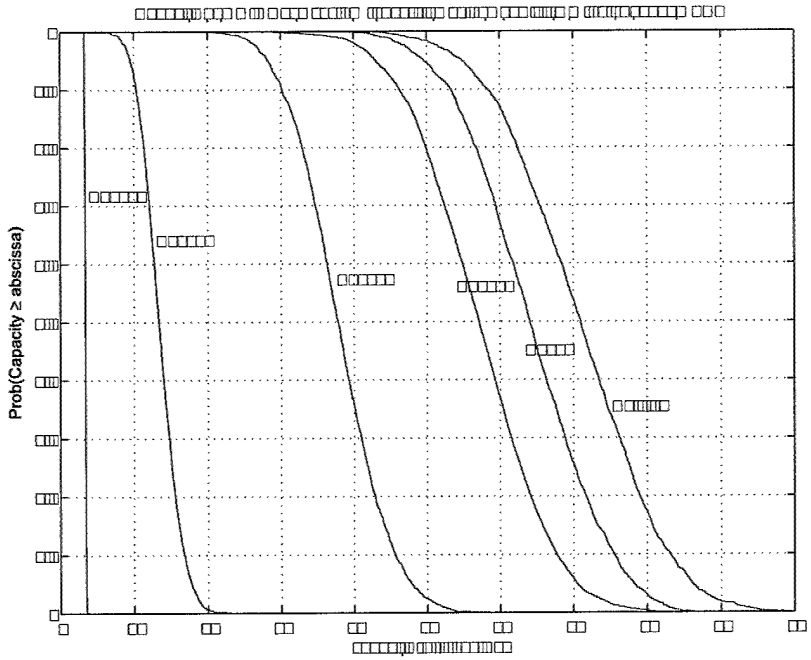

Figure 13, Capacity CCDFs for a MIMO 4x4 system at 20 dB SNR for varying values of the Rician K factor.

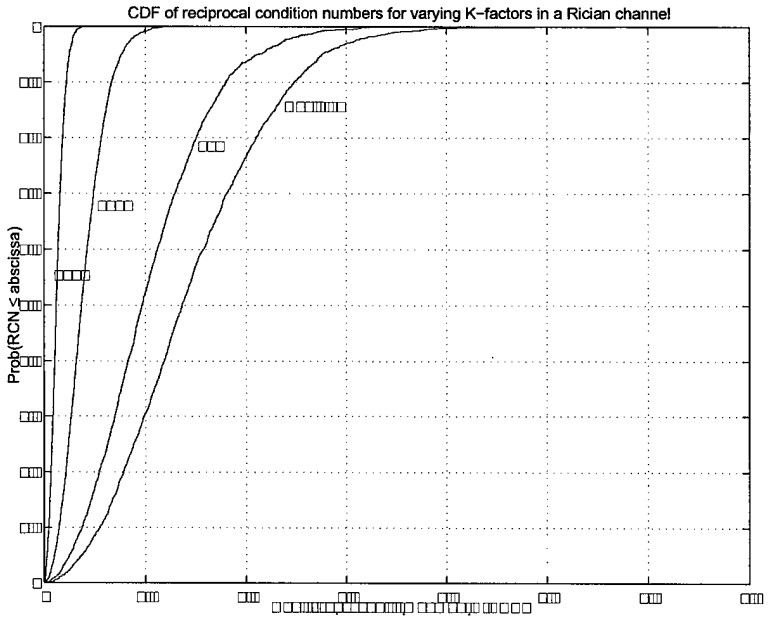

Figure 14, CDFs of Reciprocal condition numbers in a 4x4 Rician channel for varying k-factors

Figure 14, shows the distribution of the reciprocal condition number for the channels based on which the CCDFs of Figure 13 where calculated. There is a clear correlation between the reciprocal condition number which measures the ratio of the smallest eigen value of the channel matrix to its largest eigen value. In fact the capacity of the channel is inversely proportional to the reciprocal condition number.

Preliminary Simulation and Experimental Results.

In this section we provide a set of simulation results of the end to end system operating over realistic channel models, and in the presence of modelled impairments such as phase noise and IQ imbalance. Additionally we report on a set of field trials conducted using the non-real time testbed available through the wireless integrated systems research group at the university of California, Los Angeles. Rather than describing the simulation results first followed by the experimental results we have decided to show the two results concurrently on the same plots so as to provide a better means of comparing their relative performance. As is evident from the description of the testbed provided in the next section, the transmitter and receiver portions of the simulator and the experimental setup are identical. What differs is that the experimental setup includes real RF impairments, and real channel propagation effects, whereas the simulation does not. The RF impairments particularly can degrade the performance of the actual system relative to the idealized simulated system. Another major difference between the experimental and simulation results is that the AGC and block boundary detection algorithms on the testbed were implemented in real time on an FPGA. All relevant results are presented in the following subsections.

Overview of the testbed used

The architecture of the current non-real-time MIMO prototype developed at the wireless integrated systems group is illustrated in Figure 15 and a picture of the platform is shown in Figure 16. The prototype is operated through a user friendly GUI and transfers data over the air in bursts as large as 70 ms. The 70 ms real-time transmission is made possible by buffers at the transmitter and receiver. Data is modulated and de-modulated on the PC using a software that implements the baseband MIMO algorithms developed by Pulsar. Some of the features of the prototype are:

- MxN (M,N ≤2) MIMO OFDM wireless communication.;
- M-QAM modulation on OFDM sub-carrier;
- User defined packet and pilot structure, training length, and OFDM subchannel width;
- Bandwidth of 25 MHz at a carrier frequency of 5.25 GHz;

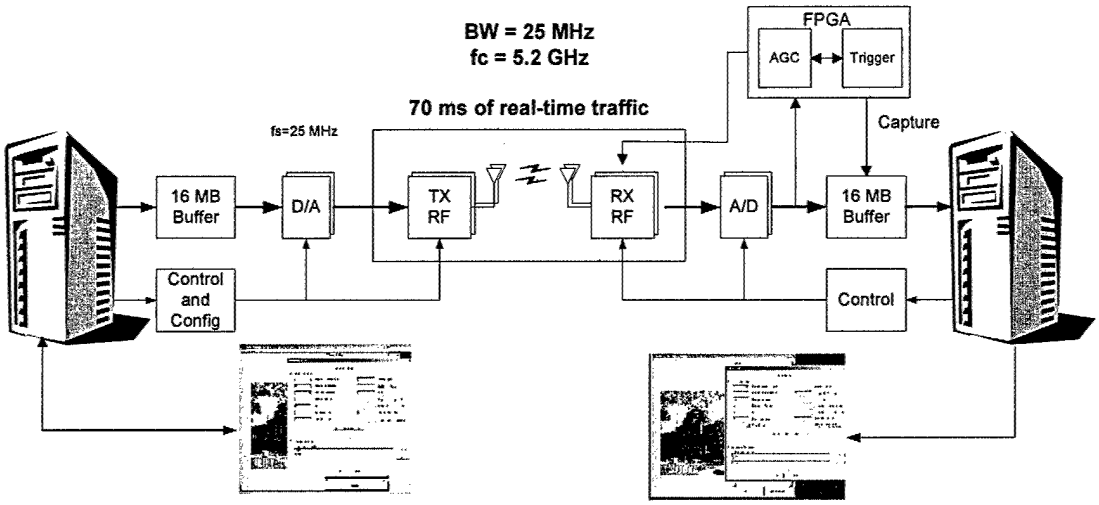

Figure 15 Architecture of Non-Real-Time MIMO Prototype

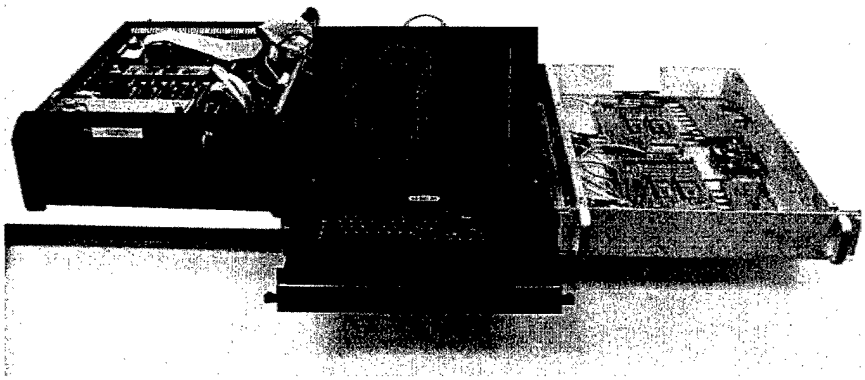

Figure 16. Picture of the MIMO Prototype

This prototype was used to study and characterize the behaviour of MIMO OFDM wireless links in several real environments as a function of different PHY parameters. Our initial efforts were to use the testbed to characterize the environment and the physical layer for point-to-point MIMO OFDM transmissions. The measurements were conducted in typical indoor environments with line-of-sight, non-line-of-sight, and corridor transmission scenarios. One aspect of the work focused on characterizing the environment and physical layer performance for scenarios where the MIMO technology is stressed. For example, the MIMO performance was studied for line-of-sight transmission with various transmitter to receiver distances and antenna separations to find the break point of MIMO communications.

However, before continuing with a description of the experimental results obtained using the testbed it is important to describe the environment were the measurements were taken. Two classes of environments where exercised. The first is an indoor setting in which both line of sight and non line of sight experiments were carried out. The second is an outdoor setting where the transmitter and receiver were place in line of sight and the separation between the antennas was changed. The building is a modern concrete office building. The internal walls have a metallic frame and are covered with sheetrock. Within this building three different experiments were conducted. In the first, the transmitter and receiver were placed in the same room, in the second, the transmitter was placed in one room and the receiver was taken to the adjoining room. In the third the transmitter was placed in one room and the receiver was moved along the hallway.

Figure 17, shows a picture of the outdoor environment where experiments were conducted. As is shown in the figure, the area is an open courtyard with very few obstructions in the vicinity of either the transmitter or the receiver. The transmitter and receiver are in line of sight of one another. At first glance the channel looks to be dominated by the line of sight component and as such extremely ill conditioned with very little hope of being able to achieve true MIMO communications. Our experiments, however, showed that with sufficient separation of the antennas at either side true MIMO communications can be accomplished (the results are presented later in this section).

Figure 17, Outdoor environment along with location of the transmit and receive antennas.

Experimental and Simulation Results

The results presented in Figure 18 compare the Cumulative Distribution Function (CDF) of the slicer-SNR for SISO, SIMO, and a 2x2 MIMO systems. These results illustrates the superiority of MIMO which can provide twice the throughput rate as a traditional SISO system for the same total transmit power and comparable outage probability for 10 dB SNR (10^{-3} BER). Once again it is important to note that the results include all the algorithms described in the previous section as well as all RF and channel impairments associated with real transmissions. Also reflected in the curves of Figure 18 is the impact of common phase error correction on the overall performance of the system. Common phase error is the term used to identify the slow variation of the oscillator phase noise. As is shown in the figure, raw performance of the testbed (without the incorporation of any phase noise cancellation algorithm in the receiver) is anywhere from 1.5 dB to as much as 4 dB off relative to the performance when phase error

cancellation is incorporated into the baseband (note that this is not the theoretical bound, but rather the performance with a phase error cancellation algorithm running in the baseband).

Figure 19 shows the same type of measurement as was reported in Figure 18, except that here the transmitter and receiver were put into adjacent rooms and the transmit power level was increased to 10 dBm. Superimposed on the same plot are the simulation results. It is important to note at this juncture that the simulator incorporated models of typical RF impairments. The figure provides a side by side comparison of the ability of the simulator to accurately predict the performance seen in the field.

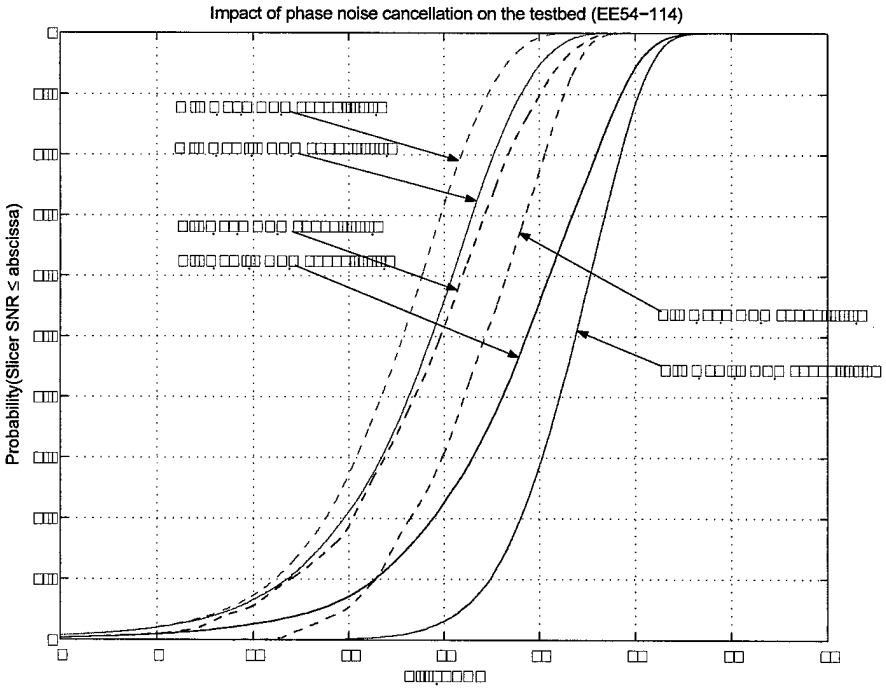

Figure 18. Indoor experimental MIMO system measurements with and without common phase error cancellation algorithms. Both TX and RX were placed in the same room. TX power equaled -3 dBm (0.5 mW).

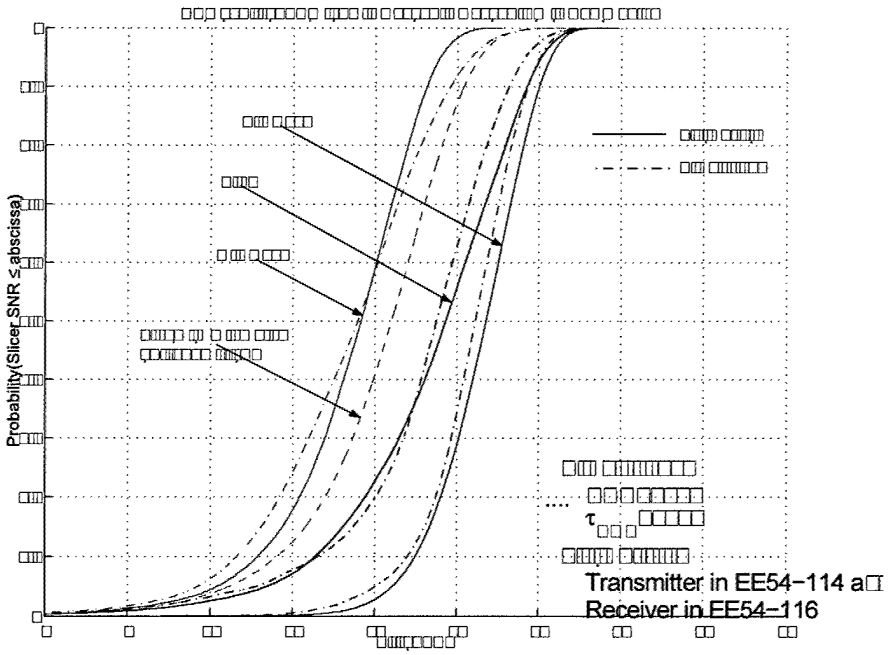

Figure 19, Comparison of experimental and simulation results for MIMO2x2, SIMO1x2 and SISO in NLOS environment.

In addition to the complementary cumulative distribution functions (CCDFs) shown in Figure 18 and Figure 19, we also investigated the achievable capacity assuming a perfect set of baseband algorithms. These numbers where derived from the slicer SNR by simply going through the widely known channel capacity equations. The trends are similar to the results of the previous measurements. The achievable capacity of a MIMO 2x2 channel is larger than that of a 1x2 which in turn is larger than that of a 1x1 SISO system. In fact 12 bps/Hz of capacity is achievable if the implementation loss at the receiver could be minimized.

The last study that we conducted was a rather quick comparison between a commercially available 802.11a card and the 2x2 MIMO testbed. We placed the transmitter unit of the testbed system in the laboratory, and placed the receiver unit on a cart and started to move down the corridor. Every 50 feet we made a measurement of the achievable user throughput (discounting the FEC overhead). We then tabulated the results, see Table 2, alongside results published by Atheros for their commercially available 802.11a chipset. The key trend to note is the ability of the MIMO system to maintain its high throughput rate as the distance is increased. At 10 feet separation the MIMO system only provides a 54% increase in throughput relative to the 802.11 system. However, the difference at 200 feet is quite compelling. In this case the MIMO system does 500% better than the 802.11a system with ¼ the overall transmit power. These early results are encouraging and point to the tremendous potential for a MIMO SDR to meet the needs of current and future military communication systems in multipath rich environments and non line of sight communications.

	Effective User throughput (Mbps)		
Distance between TX and RX (feet)	2x2 MIMO with 10mW TX power	802.11a with 45 mW TX power (source Atheros)	802.11b (source Atheros)
10'	85 Mbps	54 Mbps	11 Mbps
50'	49 Mbps	37 Mbps	11 Mbps
100'	49 Mbps	18 Mbps	11 Mbps
150'	42 Mbps	12 Mbps	6 Mbps
200'	30 Mbps	6 Mbps	2 Mbps

Table 2, throughput comparison of a MIMO 2x2 system with commercial 802.11x systems.

Summary & Future Work

The following is a list of achievements during the phase one effort:

- Identified a highly flexible SDR hardware architecture (detailed in the first progress report) with the following features
  - Dual band TDD transmission
  - Variable bandwidth (bandwidth agility)
  - Variable center frequency (frequency agility) within the prescribed bands
  - Parameterizable OFDM modulation
  - Programmable NxM MIMO configuration.
- Identified all receiver algorithms for a MIMO OFDM system (detailed in this progress report) and included them in a complete end to end sample accurate simulation platform.
- Carried out simulations to quantify the performance of the end to end system (detailed in this progress report) the simulations underscored the tremendous potential of MIMO communications for achieving high throughput rates in highly dispersive harsh environments.
- Tested our initial protocols on a non-real-time 2x2 OFDM prototype system.
- Conducted field trails in typical indoor and outdoor environments using the non-real-time testbed.
  - Demonstrated achievable spectral efficiencies of up to 12 bps with a small 2x2 configuration

- Demonstrated both indoor and outdoor applications of MIMO
- Demonstrated and quantified improvement of the proposed 2x2 system over commercially available 802.11a systems.

A possible phase 2 effort will build on this work and would deliver a complete MIMO SDR hardware platform operating in real time and delivering user data rates of as much as 0.2 Gbps in multipath rich environments. Milestones in a phase 2 study would include

- End to end C simulation of the system including the signal processing operations, the communications algorithms, and RF impairments
- Requirements for baseband and RF hardware platforms
- Complete architectural and specification of the board
- Portation of both the signal processing and communications algorithms to target FPGA platforms
- Development of the RF board
- Unit testing of the RF
- Unit testing of the transceiver baseband boards in loop back configuration
- Testing of the MIMO SDR in controlled laboratory environments (this requires the baseband and the RF to be fully operational and integrated with one another)
- Field testing of the MIMO SDR in typical urban settings in Los Angeles
- Field testing of the MIMO SDR in typical military field environments

References

[1] R. Van Nee, and R. Prasa, *OFDM for Wireless Multimedia Communications*. Artech House, 2000.

[2] G. Foschini, and M. Gans, "On Limits of Wireless Communications in a Fading Environment when Using Multiple Antennas," *Wireless Personal Communications*, vol. 6, no.3, pp. 311-335, March 1998.

[3] G. Foschini, "Layered Space-Time Architecture for Wireless Communication in a Fading Environment when Using Multi-Element Antennas," *Bell Labs Technical Journal,* vol. 1, no. 2, pp. 41-59, Fall 1996.

[4] J. Tierney, C.M. Rader, B.A. Gold, "Digital frequency synthesizer," *IEEE Transactions on Audio and Electroacoustics*, vol.Au-19, no.1, p.48-57, March 1971.

[5] A.L. Bramble, "Direct digital frequency synthesis," *Proceedings of the Thirty Fifth Annual Frequency Control Symposium*, p.406-14, 1981.

[6] D.P. Noel, T.A. Kwasniewski, "Frequency synthesis: A comparison of techniques,"*Proceedings of Canadian Conference on Electrical and Computer Engineering*, Canada, vol.2, p.535-8 Sept.1994.==

[7] L.K. Tan, H. Samueli, "200 MHz quadrature digital synthesizer/mixer in 0.8μm CMOS," *IEEE Journal of Solid-State Circuits*, vol.30, no.3, p.193-200, March 1995.

[8] B.H. Hutchision, Jr., *Frequency Synthesis and Applications*. New York: IEEE Press, 1975.

[9] Bellaouar, M.S. O'brecht, A.M. Fahim, M.I. Elmasry," Low-power direct digital frequency synthesis for wireless communications," *IEEE Journal of Solid-State Circuits*, vol.35, no.3, p.385-90, March 2000.

[10] J.M.P. Langlois, D. Al-Khalili, "Hardware optimized direct digital frequency synthesizer architecture with 60 dBc spectral purity, "*in Proc. of IEEE International Symposium on Circuits and Systems*, vol.5, pp. 361-64, 2002.

[11] A. H. Sayed, "Fundamentals of Adaptive Filtering" John Wiley, June 2003.

[12] B. Razavi, "RF Microelectronics" Prentice Hall, 1998.

[13] D. B Leeson, "A simple model of feedback oscillator noise spectrum" Proceeding of the IEEE, Vol. 54, Feb. 1996, pp. 329-330.

[14] J-F. Frigon, B. Daneshrad, J. Putnam, E. Berg, R. Kim, T. Sun, H. Samueli "Field Trial Results for High-Speed Wireless Indoor Data Communications" IEEE Journal on Selected Areas in Communications, Vol. 18, No. 3, March 2000.

[15] R. J. Castle, A. E. Jones, T. A. Wilkinson, "An Experimental Study of OFDM at 5.25GHz in an Office Environment" IEEE Journal on Selected Areas in Communication, Vol. 19, No. 11, November 2001.

[16] F. Tufvesson, O. Edfors, M. Faulkner, "Time and Frequency Synchronization for OFDM using PN-Sequence Preambles" VTC-1999/Fall, vol 4, pp.2203-7, New Jersey, 1999.

[17] F. Classen, H. Meyr, "Frequency Synchronization Algorithms for OFDM Systems Suitable for Communications over Frequency Selective Fading Channels" pp 1655-1659, VTC June 1994.

[18] H. Nogami, T. Nagashima, □A Frequency and Timing Period Acquisition Technique for OFDM Systems□ PIMRC 1995, pp 1010-1015, Sep 27-29, 1995.